

Microstructural dependence of electron and hole transport in low-temperature-grown polycrystalline-silicon thin-film solar cells

Takuya Matsui, Riza Muhida, Tomohiro Kawamura, Toshihiko Toyama, Hiroaki Okamoto, Tsutomu Yamazaki, Shinya Honda, Hideyuki Takakura, and Yoshihiro Hamakawa

Citation: *Applied Physics Letters* **81**, 4751 (2002); doi: 10.1063/1.1527979

View online: <http://dx.doi.org/10.1063/1.1527979>

View Table of Contents: <http://scitation.aip.org/content/aip/journal/apl/81/25?ver=pdfcov>

Published by the [AIP Publishing](#)

Articles you may be interested in

[Impact of the n⁺ emitter layer on the structural and electrical properties of p-type polycrystalline silicon thin-film solar cells](#)

J. Appl. Phys. **114**, 134505 (2013); 10.1063/1.4823811

[Chemical speciation at buried interfaces in high-temperature processed polycrystalline silicon thin-film solar cells on ZnO:Al](#)

J. Appl. Phys. **113**, 044519 (2013); 10.1063/1.4789599

[N/I buffer layer for substrate microcrystalline thin film silicon solar cell](#)

J. Appl. Phys. **104**, 104505 (2008); 10.1063/1.3021053

[Defect density and recombination lifetime in microcrystalline silicon absorbers of highly efficient thin-film solar cells determined by numerical device simulations](#)

J. Appl. Phys. **94**, 1035 (2003); 10.1063/1.1577813

[Local characterization of electronic transport in microcrystalline silicon thin films with submicron resolution](#)

Appl. Phys. Lett. **74**, 1475 (1999); 10.1063/1.123585



Microstructural dependence of electron and hole transport in low-temperature-grown polycrystalline-silicon thin-film solar cells

Takuya Matsui,^{a)} Riza Muhida, Tomohiro Kawamura, Toshihiko Toyama,
and Hiroaki Okamoto

*Department of Physical Science, Graduate School of Engineering Science, Osaka University, Toyonaka,
Osaka, 560-8531, Japan*

Tsutomu Yamazaki, Shinya Honda, Hideyuki Takakura, and Yoshihiro Hamakawa

Department of Photonics, Ritsumeikan University, Kusatsu, Shiga, 525-8577, Japan

(Received 5 April 2002; accepted 16 October 2002)

Carrier transport properties of undoped polycrystalline silicon (poly-Si) thin films prepared by $\text{SiH}_4\text{-H}_2$ plasma at low temperature have been investigated. The ac-conductivity measurement technique has been applied to poly-Si *i* layers with an *n-i-n* junction structure in order to characterize the electron conductivity along the growth direction. Furthermore, the hole conductivity has been measured with *p-i-p* junction structures. The temperature dependence of ac conductivity reveals that poly-Si films with relatively low crystalline volume fraction ($X_c \sim 50\%$) exhibit intrinsic character, while the poly-Si films with high $X_c (> 50\%)$ exhibit *n*-type character with activation energies less than 0.15 eV. Based on these results, the relationship among microstructure, carrier transport, and photovoltaic performance of poly-Si solar cells is discussed. © 2002 American Institute of Physics. [DOI: 10.1063/1.1527979]

Low-temperature-grown polycrystalline silicon (poly-Si) thin films produced by plasma-enhanced chemical vapor deposition (PECVD) are currently attracting considerable attention as a low-cost and stable photovoltaic material.^{1–5} Recently, several groups have reported that poly-Si films prepared under various conditions in the PECVD process show a wide variety of microstructures from a crystalline-amorphous mixed state to an almost perfect crystalline state with different crystallographic orientations.^{2,3,5} These structural changes directly affect the carrier transport property which plays a dominant role in determining the photovoltaic performance. Due to such complicated microstructures, however, it is not straightforward to explore the carrier transport properties of poly-Si films. Moreover, little effort has been made to identify the effect of carrier transport on the photovoltaic performance.^{6,7}

For the case of the columnar grains oriented perpendicularly to substrate, which is often encountered in (220) preferentially orientated poly-Si films, the carrier transport can be separated into two components; one is along the film (parallel) and another is along the growth direction (perpendicular). In this case, the parallel conductivity should be strongly affected by the grain boundaries, whereas the perpendicular conductivity is affected very little. For the PECVD produced poly-Si films, such an anisotropic electrical transport has been reported by Kočka *et al.*⁸ Concerning practical *p-i-n* poly-Si solar cells, such carrier transport parameters as electrical conductivity of poly-Si films should be characterized in the form of sandwich electrode geometry, as in solar cell structure, because the perpendicular carrier transport clearly dominates the device operation, rather than the parallel transport. With the sandwich electrode geometry, e.g., metal/poly-

Si/metal, however, one does not observe the simple linear Ohm's law in dc current–voltage characteristics due to the presence of carrier depletion acting as a contact barrier at metal/poly-Si interfaces. The ac-conductivity measurement technique has been proposed as a powerful tool for measuring the material conductivity with a sandwich electrode geometry.⁸ In this letter, we report on the results of electrical conductivities due to electrons and holes in the poly-Si films using the ac-conductivity technique. We show that the Fermi energy level and photosensitivity in the poly-Si layer are quite sensitive to the film microstructure. Based on these results, we discuss the relationship between electrical properties and photovoltaic performance of poly-Si films.

The solar cells prepared in this work have a structure of Ag-grid/ZnO/*p-i-n*/ZnO/Ag/glass.⁵ Highly conductive microcrystalline silicon *p* and *n* layers that were deposited by a rf-PECVD system. The poly-Si *i* layers were deposited at 180 °C by another PECVD system with a very high frequency (VHF) excitation source (100 MHz). A mixture of SiH_4 and H_2 with a H_4 concentration of 4.5% was used for the growth of the poly-Si *i* layer. The film crystallinity was changed by deposition pressure in VHF-PECVD process.⁵ The crystalline volume fraction, X_c , and crystallographic orientation were determined by Raman and x-ray diffraction (XRD) measurements, respectively.⁵

The ac-conductivity measurement was performed on 2- μm -thick poly-Si *i* layers with different sample structures consisting of ZnO/*n-i-n*/SnO₂/glass and ZnO/*p-i-p*/SnO₂/glass. The flat ZnO and SnO₂ films were employed as front and rear side transparent electrodes, respectively. The dark ac conductivity was measured in the frequency range of 50 Hz–1 MHz under an applied ac voltage of 10 mV_{rms}. Since the ac-conductivity spectra involve the effects of carrier depletion at contacts and electrode resistance, the true

^{a)}Present address: National Institute of Advanced Industrial Science and Technology, Japan; electronic mail: t-matsui@aist.go.jp

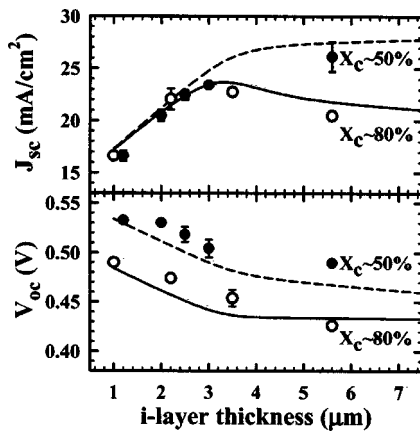


FIG. 1. Short circuit current density (J_{sc}) and open circuit voltage (V_{oc}) of poly-Si solar cells with different i -layer crystalline volume fractions of $X_c \sim 50\%$ (closed) and $\sim 80\%$ (open) as a function of i -layer thickness. Dashed and solid lines represent theoretical plots calculated with $S_{GB} = 10$ cm/s, $N_{GB} = 10^{13}$ cm $^{-3}$ (model A) and $S_{GB} = 20$ cm/s, $N_{GB} = 10^{16}$ cm $^{-3}$ (model B), respectively.

film conductivity of poly-Si i layer can be determined at frequencies where the relative permittivity, ϵ_{eff} , approaches a proper value of $\epsilon_{eff}(Si) = (Cd/\epsilon_0 S) \approx 12$.⁸ Here, C , d , ϵ_0 , and S denote the capacitance corresponding to the imaginary part of measured admittance spectra, the sample thickness, the vacuum permittivity, and the sample area, respectively. The photoconductivity was also measured under air mass 1.5, 100 mW/cm 2 illumination through the glass substrate.

Figure 1 shows the short circuit current density, J_{sc} , and open circuit voltage, V_{oc} , of poly-Si solar cells as a function of i -layer thickness in the range of 1.0–5.6 μ m. In Fig. 1, the results on poly-Si with $X_c \sim 50\%$ are compared to those on poly-Si with $X_c \sim 80\%$. Both series of poly-Si layers exhibit (220) preferential orientation.⁵ The solid and dashed lines in Fig. 1 represent the theoretical fits which will be discussed later. Regardless of X_c , J_{sc} linearly increases with increasing thickness up to the i layer thickness of 3 μ m. No significant difference is found for the improvement in J_{sc} between solar cells with X_c of $\sim 50\%$ and $\sim 80\%$. However, J_{sc} rapidly starts to decrease at the thickness above 3 μ m for $X_c \sim 80\%$, whereas J_{sc} gradually increases at the thickness above 5 μ m for $X_c \sim 50\%$. On the other hand, V_{oc} significantly decreases with an increase in the i -layer thickness. In particular, independent of i -layer thicknesses, V_{oc} for $X_c \sim 80\%$ is always lower than that for $X_c \sim 50\%$. It is evident that the poly-Si layer with $X_c \sim 50\%$ is advantageous as the photovoltaic material in comparison with that with $X_c \sim 80\%$. In fact, using the poly-Si i layer with $X_c \sim 50\%$, a maximum conversion efficiency of 9.18% ($J_{sc} = 25.1$ mA/cm 2 , $V_{oc} = 0.527$ V, fill factor = 0.7) has been achieved with the i -layer thickness of 2.5 μ m, by employing an appropriate light trapping structure.⁹

In order to elucidate the relationship between poly-Si microstructure and photovoltaic performance, electrical characterization was performed on poly-Si films by the conductivity technique. In Fig. 2, the temperature dependence of dark conductivity (σ_d) measured for poly-Si i layers with different crystalline volume fractions ($X_c \sim 50\%$ and $\sim 80\%$) is shown. Figure 2 also demonstrates σ_d measured for the n - i - n and the p - i - p samples. It should be

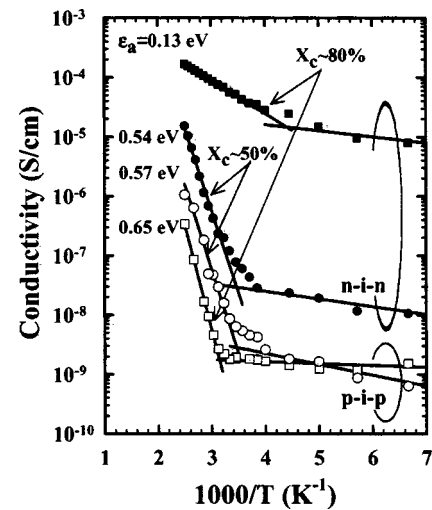


FIG. 2. Temperature dependence of dark conductivity of poly-Si i layers with different crystalline volume fractions of $X_c \sim 50\%$ (circles) and $\sim 80\%$ (squares) measured with n - i - n (closed) and p - i - p (open) sample structures.

noted that poly-Si i layers in the n - i - n and p - i - p samples are generally expected to be different due to the difference in the nucleation behavior on n and p layers. Nevertheless, in this series, no significant structural difference is found between poly-Si i -layer deposited on n layer and that on p layer from the Raman and XRD measurements. In Fig. 2, a remarkable difference in the dark conductivity behaviors is observed for these two poly-Si i layers. For the poly-Si film with $X_c \sim 50\%$, the activation energies of the dark conductivity, ϵ_a , which is deduced from the Arrhenius plot in the higher temperature regime (300–400 K), are almost identical around 0.55 eV for both n - i - n and p - i - p samples. For the poly-Si film with $X_c \sim 80\%$, on the other hand, ϵ_a for n - i - n is much smaller than that for p - i - p . These electrical properties depending on sample structures can be interpreted as follows. For the n - i - n sample, the n/i interfaces should act as barriers for the hole extraction, and only electrons can contribute to the current flow if the applied voltage is much smaller than the barrier height impeding hole extraction. On the contrary, the p - i - p sample permits only holes for the current flow. Since the activation energy of the dark conductivity is a good measure of the Fermi energy from the band edge for the carrier transport, the result on the poly-Si film with $X_c \sim 50\%$, i.e., $\epsilon_a \sim 0.55$ eV being independent of sample structure suggests that the Fermi level locates at the center of the band gap. Thus, this material is almost intrinsic. For the poly-Si film with $X_c \sim 80\%$, on the other hand, the small ϵ_a for electron transport and the large ϵ_a for hole transport provide strong evidence that the Fermi level is close to the conduction band edge. Thus, this material is n type. Table I summarizes room temperature σ_d taken from the Arrhenius plot shown in Fig. 2, together with the results of photoconductivity (σ_{ph}) and photosensitivity (σ_{ph}/σ_d). In Table I, σ_{ph} is less dependent on poly-Si crystallinity compared to σ_d , implying that σ_{ph} is determined by the number of photogenerated carriers under light illumination, rather than by the Fermi level at thermal equilibrium. Accordingly, σ_{ph}/σ_d is predominantly determined by σ_d . In particular, σ_{ph}/σ_d is markedly varies with sample structure. As a result, σ_{ph}/σ_d for p - i - p is found

TABLE I. Dark conductivity (σ_d), photoconductivity (σ_{ph}), and photosensitivity (σ_{ph}/σ_d) of poly-Si *i* layers with different crystalline volume fractions (X_c) measured with *n-i-n* and *p-i-p* sample structures.

X_c (%)	<i>n-i-n</i> (<i>p-i-p</i>)	σ_d (S/cm)	σ_{ph} (S/cm)	σ_{ph}/σ_d
~50	<i>n-i-n</i>	1.7×10^{-7}	5.8×10^{-5}	3.4×10^2
	(<i>p-i-p</i>)	8.3×10^{-9}	1.5×10^{-6}	1.8×10^2
~80	<i>n-i-n</i>	4.1×10^{-5}	1.1×10^{-4}	2.7
	(<i>p-i-p</i>)	3.8×10^{-10}	5.4×10^{-6}	1.4×10^4

to be much higher than that for *n-i-n*, where σ_{ph}/σ_d differs by four orders magnitude. This result provides additional support that photogenerated holes dominate minority carrier transport in the highly crystallized poly-Si films.

It has been reported that the origin of earlier-mentioned *n*-type character observed in highly crystallized poly-Si films is attributed either to intrinsic nature or to the electrically active oxygen-related complex.^{2,10–12} In general, it is widely accepted that the oxygen-related donors concentrate at grain boundaries in the poly-Si films,¹¹ and oxygen contaminated grain boundaries give rise to similar defect energy distribution as Si/SiO₂ interface.¹² This idea of such an electrically activated grain boundaries with high donor concentration in the poly-Si films allows us to give clear explanations for the results of the thickness dependence of photovoltaic performance shown in Fig. 1. The lines shown in Fig. 1 represent calculated results based on the two-dimensional grain boundary model¹³ in which uniform columnar grains in the *i* layer with lateral grain size of 0.01 μm are assumed. Here, the dashed lines (model A: intrinsic) indicate simulation results calculated with the surface recombination velocity at grain boundary of $S_{GB}=10$ cm/s and the effective donor concentration at grain boundary of $N_{GB}=10^{13}$ cm⁻³. For the solid line (model B: *n* type) $S_{GB}=20$ cm/s and $N_{GB}=10^{16}$ cm⁻³ are assumed. Preliminary studies^{13,14} have suggested that S_{GB} should be lower than 100 cm/s in order to reproduce recent experimental results of poly-Si solar cells. N_{GB} values given in models A and B are set as their macroscopic dark conductivities to be identical with the measured dark conductivities for $X_c \sim 50\%$ and $\sim 80\%$, respectively. Figure 3 shows the calculated carrier recombination rate along the grain boundary position for both cases of models A and B, at short circuit condition ($V=0$ V) and at forward biased condition ($V=0.43$ V). The *i*-layer thickness is set at 5.0 μm . Under short circuit condition, carrier recombination rate in model B is much higher than that in model A particularly at an *i*-layer position adjacent to *i/n* interface. The considerable recombination loss of photogenerated carriers found in model B is ascribed to the higher S_{GB} and to the lower built-in electric field in the *i* layer due to *n*-type character. This calculation result is consistent with the measured spectral response. In the solar cells with $X_c \sim 80\%$, the rapid decrease in J_{sc} at the thickness >3 μm arises from the significant decrease in the quantum efficiencies at longer wavelengths (>600 nm). Since the long wavelength response is mostly determined by the diffusion length of minority carriers generated at rear side of the solar cell, it can be interpreted as that the photogenerated holes are no longer collected effectively if the cell thickness exceeds 3 μm .

The situation is quite different at $V=0.43$ V at which

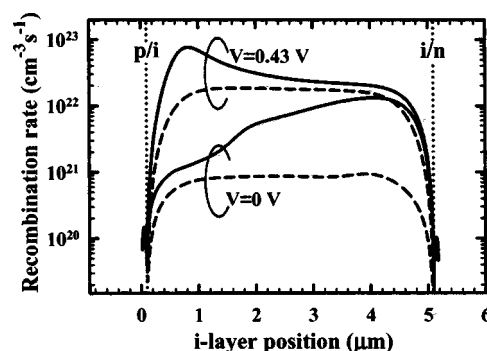


FIG. 3. Calculated carrier recombination rate profiles along the grain boundary position, at short circuit condition ($V=0$ V) and at forward biased condition ($V=0.43$ V). Dashed and solid lines represent the calculation results using $S_{GB}=10$ cm/s, $N_{GB}=10^{13}$ cm⁻³ (model A) and $S_{GB}=20$ cm/s, $N_{GB}=10^{16}$ cm⁻³ (model B), respectively.

forward applied voltage is nearly close to open circuit condition. In Fig. 3, model B reveals that the intensive carrier recombination takes place near the *p/i* interface when $V=0.43$ V. Due to its *n*-type character, the built-in electric field locally concentrates at *p/i* interface. Therefore, carrier density at this depletion region is dramatically increased by the forward bias application. Since the recombination rate is determined by the product of majority carrier density and minority carrier density, holes recombine with “majority” electrons at the *p/i* interface via the defective grain boundaries. This effect would account for the finding that V_{oc} for $X_c \sim 80\%$ is always lower than that for $X_c \sim 50\%$.

In conclusion, we demonstrate that the ac-conductivity measurement with *n-i-n* and *p-i-p* sample structures can be applied to determine the individual electron and hole conductivities along the poly-Si growth direction. The poly-Si films with relatively low crystalline volume fraction $X_c \sim 50\%$ exhibit intrinsic character, leading to the successful high efficiency solar cell fabrication. In contrast, poly-Si films with high crystalline volume fraction induce higher film conductivity with *n*-type character. This effect is proposed to be responsible for the pronounced reduction in V_{oc} .

¹ K. Yamamoto, IEEE Trans. Electron Devices **46**, 2041 (1999).

² H. Keppner, J. Meier, P. Torres, D. Fischer, and A. Shah, Appl. Phys. A: Mater. Sci. Process. **69**, 169 (1999).

³ O. Vetterl, R. Carius, L. Houben, C. Scholten, M. Luysberg, A. Lambertz, F. Finger, and H. Wagner, Mater. Res. Soc. Symp. Proc. **609**, A15 (2000).

⁴ Y. Nasuno, M. Kondo, and A. Matsuda, Jpn. J. Appl. Phys., Part 2 **40**, L303 (2001).

⁵ T. Matsui, M. Tsukiji, H. Saika, T. Toyama, and H. Okamoto, Jpn. J. Appl. Phys., Part 1 **41**, 20 (2002).

⁶ M. Goerlitzer, P. Torres, N. Beck, N. Wyrsh, and A. Shah, J. Non-Cryst. Solids **227–230**, 996 (1998).

⁷ O. Vetterl, A. Groß, T. Jana, S. Ray, A. Lambertz, R. Carius, and F. Finger, J. Non-Cryst. Solids **299–302**, 772 (2002).

⁸ J. Kočka, A. Fejfar, V. Vorlíček, H. Stuchlíková, and J. Stuchlík, Mater. Res. Soc. Symp. Proc. **557**, 490 (1999).

⁹ T. Matsui, M. Tsukiji, H. Saika, T. Toyama, and H. Okamoto, J. Non-Cryst. Solids **299–302**, 1152 (2002).

¹⁰ S. Vepřek, Z. Iqbal, R. O. Kühne, P. Capezuto, F. A. Sarott, and J. K. Gimzewski, Solid State Phys. **16**, 6241 (1983).

¹¹ Y. Nasuno, M. Kondo, and A. Matsuda, Appl. Phys. Lett. **78**, 2330 (2001).

¹² J. H. Werner, Inst. Phys. Conf. Ser. **104**, 63 (1989).

¹³ T. Matsui, T. Yamazaki, A. Nagatani, K. Kino, H. Takakura, and Y. Hamakawa, Sol. Energy Mater. Sol. Cells **65**, 87 (2001).

¹⁴ J. H. Werner, Technical Digest of 13th Sunshine Workshop on Thin Film Solar Cells (NEDO, Tokyo, 2000), p. 41.